Influence of experimental conditions on the spectroscopy investigation of ^{14}Be by Coulomb breakup reaction *

Yu-Shou Song(宋玉收)[1)] Ying-Wei Hou(侯英伟) Li-Yuan Hu(胡力元) Hui-Lan Liu(刘辉兰)
Hong-Yi Wu(吴弘毅)

Key Discipline Laboratory of Nuclear Safety and Simulation Technology, Harbin Engineering University, Harbin 150001, China

Abstract: The two-body (core+2n) cluster structure was implemented to describe the two-neutron halo nucleus ^{14}Be, where the core ^{12}Be was assumed inert and at a ground state and the dineutron was assumed at a pure $2S_0$ state. Based on such a structure the three-body continuum-discretized coupled-channel (CDCC) calculation was successfully used to deal with the ^{14}Be breakup reactions of ^{14}Be+Pb at 35 MeV/u. Consequently, we modeled the kinematically complete measurement experiment of this reaction with the help of Geant4. With the simulation data the relative energy spectrum was constructed by the invariant mass method and B(E1) spectrum was extracted using the virtual photon model. The influence of the target thickness and detector performance on the energy spectroscopy was investigated.

Keywords: Coulomb breakup, halo nucleus, dineutron, spectroscopy

PACS: 25.70.De, 29.30 **DOI:** 10.1088/1674-1137/40/5/056203

1 Introduction

Since the nuclear halo structure was discovered in 1985 [1], it has attracted much attention from nuclear physicists [2–6]. Besides the large nuclear matter radius and the narrow transverse momentum distribution of the core [3], the anomalously large Coulomb breakup cross section is another halo manifestation. With the ongoing development of radioactive ion beam (RIB) facilities and experimental techniques, kinetically complete measurement of the Coulomb breakup together with invariant mass spectroscopy has become a standard research approach of halo nucleus properties. Through the investigations of one-neutron halo nuclei like ^{11}Be [4], ^{15}C [7], it has been discovered that the cross section enhancement is due to the spatial decoupling of the halo relative to the core. A direct breakup mechanism was concluded according to the B(E1) spectrum analysis. There are similar soft Coulomb excitations for two-neutron halo nuclei, such as ^{6}He [8], ^{11}Li [9] and ^{14}Be [10]. The understanding of the nature of the E1 excitation for two-neutron halo nuclei depends on experimental investigation of their energy spectra. However, the experiments are more complicated and difficult to carry out than with one-neutron halo nuclei. The inefficiency of correlated two-neutron detection and the thin target approximation may lead to distorted energy spectra, which was indicated in the ^{11}Li [9] relative spectrum measurement.

In order to discover how the experimental setting influences the energy spectroscopy of ^{14}Be Coulomb breakup on a Pb target, the kinetically complete measuring experiment was modeled with the help of the Geant4 Monte Carlo toolkit [11]. The transportation of the projectile and outgoing particles were handled by Geant4-provided physical processes. To deal with the breakup of a two-neutron halo nucleus, a so-called four-body CDCC, including a three-body projectile [12] and a target, was developed independently by two groups [13, 14]. However, such a calculation is still at a primary phase and has principally achieved success so far in calculating the reactions of ^{6}He. According to the theoretical structure investigation of two-neutron halo nuclei, the dineutron correlation plays a dominant role [15, 16]. Therefore, in this report the Coulomb breakup of ^{14}Be is studied by the so-called three-body CDCC [17] calculation (FRESCO code), with a two-body projectile (^{12}Be+dineutron) and a target nucleus. The theoretical results of the energy spectrum and the angular distribution of a single neutron agree with the exist experimental data. Based on the data output of the simulated experiment, the relative kinetic energy spectrum are reconstructed by the invariant mass method, and consequently the B(E1) spectrum is extracted by the virtual photon model of electromagnetic dissociation (EMD) [18]. The influence of

Received 29 September 2015

∗ Supported by National Natural Science Foundation of China (11205036)

1) E-mail: songyushou80@163.com

the target thickness and the performance of the detector system behind the target on the energy spectroscopy is discussed.

2 The breakup reaction of ^{14}Be

The breakup process of ^{14}Be on a high Z target (Pb) consists of two parts — the structure part and reaction part. For the structure, ^{14}Be was treated as a ^{12}Be core plus a dineutron with a spin of zero [19–21]. According to the Pauli principle, NL of the dineutron equals $2S$. Ignoring the internal motion of the dineutron, the binding energy between ^{12}Be and the dineutron is taken as the two-neutron separation energy S_{2n} for the ground state. The distance between ^{12}Be and the dineutron was set as 5.6(9) fm according to the calculation with a few-body reaction model for ^{14}Be [22]. Only the first 2^+ resonance state at excitation energy 1.54(13) MeV, i.e. at 0.27 MeV above the breakup threshold, was taken into account [23, 24]. Assuming ^{14}Be and the core ^{12}Be both lie in the ground state, the Woods-Saxon potential with the parameters listed in Table 1 was implemented to calculate their wave functions. The first 2^+ state has the same potential parameters except the depth of the binding potential V_0, which was adjusted according to the excited energy.

Table 1. The Woods-Saxon potential parameters for ground state and first 2^+ state of two-body ^{14}Be.

	a_1	a_2	r_c/ fm	V_0/ MeV	r_0/ fm	a_0/ fm
^{14}Be$_{g.s.}$	0	12	1.2	38.85	1.81	0.65
^{14}Be$_{2+}$	0	12	1.2	35.28	1.81	0.65

The three-body CDCC method was implemented to deal with the breakup reaction of ^{14}Be. For the breakup of ^{14}Be on a Pb target, the Coulomb force is dominant. Referring to the one-neutron halo nuclei, it was assumed to be a direct reaction. Therefore, only s wave and p wave were taken into account, while d and above orders that include resonance states were ignored. As for the optical potential between the outgoing particles and the target nucleus, the potential between ^{12}Be and ^{208}Pb was substituted by ^{13}C+^{208}Pb [25] and the potential of 2n+^{208}Pb was substituted by that of d+^{208}Pb [26]. Considering the Coulomb interaction exclusively and fixing the normalizing factor as 0.27, the relative energy spectrum obtained is as shown in Fig. 1, which agrees well with the experimental result from Labiche et al [10].

In the following we will consider how the initial kinetic states of the outgoing particles should be given in the Monte Carlo code. The breakup process is split into two steps, the inelastic scattering of ^{14}Be and the breakup of the excited ^{14}Be*

$$^{14}\mathrm{Be}+\mathrm{Pb} \rightarrow {}^{14}\mathrm{Be}^*+\mathrm{Pb}', \quad (1)$$

$$^{14}\mathrm{Be}^* \rightarrow {}^{12}\mathrm{Be}+\mathrm{n}+\mathrm{n}. \quad (2)$$

In the first step, the incident channel was determined according to the experiment setting. For the outgoing channel, the rest mass of ^{14}Be* satisfies $M(^{14}\mathrm{Be}^*) = E_x + M(^{14}\mathrm{Be})$, where the excited energy can be written as the sum of the relative energy of the three outgoing particles and the $2n$ separation energy of ^{14}Be

$$E_x = E_{\mathrm{rel}} + S_{2n}. \quad (3)$$

The 2n separation energy $S_{2n} = 1.27(13)$ MeV [27] is a constant. The relative energy spectrum (Fig. 1) and angular distribution (Fig. 2(a)) of ^{14}Be* were given by the theoretical calculation using the CDCC method. According to energy and momentum conservation in this step the momentum of ^{14}Be* was generated.

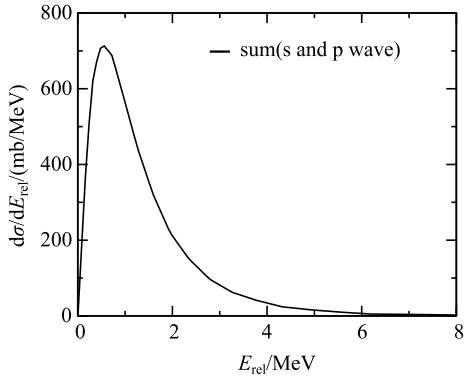

Fig. 1. The calculated relative energy spectrum of ^{14}Be Coulomb excitation on a Pb target. In the CDCC calculation, the core+2n structure was assumed.

In the center of mass (c.m.) system of the outgoing particles the relative kinetic energy taken by ^{12}Be is expressed as $E_{\mathrm{rel},^{12}\mathrm{Be}} = kE_{\mathrm{rel}}$, where k is the relative energy partition coefficient varying from 0 to 1 and was assumed to obey a uniform distribution. The relative energy taken by the two-neutron system $E_{\mathrm{rel,n+n}} = (1-k)E_{\mathrm{rel}}$ according to energy conservation. The differential cross section of the ^{12}Be is uniform since there is no direction specific in this c.m system. Hence, the momentum of ^{12}Be can be generated and the momentum of the two-neutron system determined by momentum conservation. For the same reason as ^{12}Be, the direction of the flying neutron is also isotropic in the c.m. system of n+n. In the same way the momenta of the two neutrons are generated. Consequently, through performing one and two Lorentz transformations respectively the initial momenta of the ^{12}Be and the two neutrons in the laboratory system were obtained. The single-neutron angular distribution is in Fig. 2(b), which is consistent with the experimental result of [10].

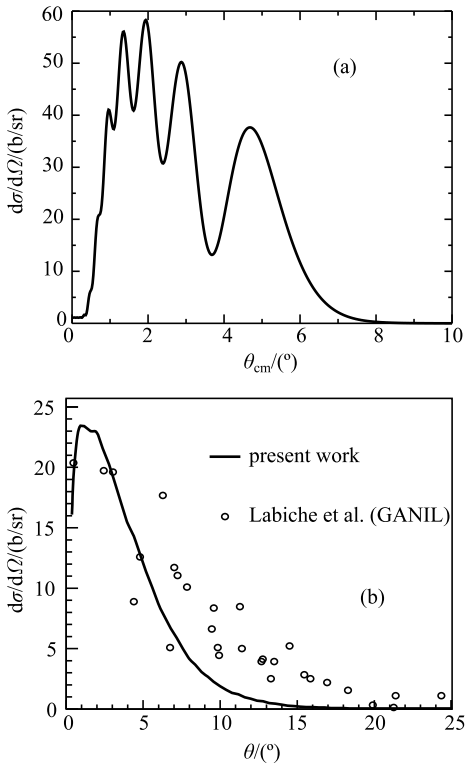

Fig. 2. (a) The angular distribution of the scattered ^{14}Be* in the c.m system of ^{14}Be+Pb given by theoretical calculation. (b) The single-neutron angular distribution in the laboratory system from experiment [10] (circles) and our simulation (solid line).

3 Modeling of the experiment

Geant4 provides seven major categories of physical processes which may be encapsuled in different modular physics lists. Some standard physics lists are given for general application in the release package. In our simulation workspace, Geant4 (version 4.10.00) was used and "QGSP_BERT_HP" was selected as the physics list. In this physics list, the thermal neutron interaction with the scintillator is handled by the data driven high precision neutron (HP) package; a standard electromagnetic (EM) process builder covering ionisation, bremsstrahlung, Coulomb scattering etc. is implemented to deal with EM interactions. To improve the simulation accuracy of slow charged particles, a process builder based on PENELOPE [28] was introduced to replace the standard one. The Coulomb breakup of ^{14}Be on a Pb target as described above was made into a discrete process and added into the physics list "QGSP_BERT_HP". To improve the computing efficiency of scintillation, we recorded the electron equivalent energy deposition [29] instead of processing the scintillation photons.

There are convenient and flexible geometric modeling approaches in the Geant4 toolkit. The geometry of the experimental apparatus (without magnetic dipole) for ^{14}Be Coulomb breakup was modeled as is schematically exhibited in Fig. 3. The double-side silicon strip (SSD) thickness of 1000 microns was chosen and the CsI cross section was 2 cm×2 cm (the thickness is set according to the incident energy). They were placed 20 cm and 50 cm behind the target respectively to form a charged ion telescope responsible for outgoing fragments detection. The neutron wall was placed five meters behind the target. It included five layers of plastic scintillator (BC408) bars with a separation between adjacent layers of 6 cm. The configuration is as described in Ref. [30]. The cross section of each bar is 6 cm×6 cm; the number of bars in each layer and the length of the bar are set according to the angular coverage requirement.

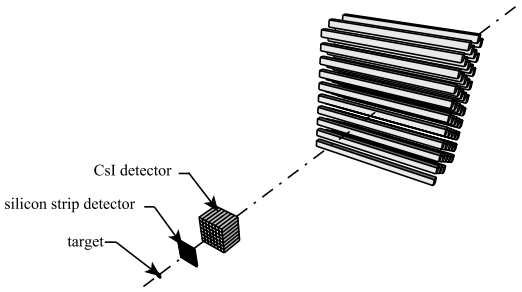

Fig. 3. The schematic layout of the experimental apparatus for kinematically complete measurement of ^{14}Be Coulomb breakup.

4 Data analysis

In comparison with the missing mass method, the invariant mass method has much higher energy resolution in RIB experiments. Therefore, this method is widely implemented in Coulomb breakup reaction experiments of neutron halo nuclei [9, 10]. Reconstructing the four dimensional momenta of the outgoing particles the invariant mass $M(^{14}\mathrm{Be})$ of the excited ^{14}Be is expressed as

$$\begin{aligned} M(^{14}\mathrm{Be}^{*}) &= \left[\left(\sum_i E_i\right)^2 - \left(\sum_i \boldsymbol{P}_i\right)^2\right]^{1/2} \\ &= \Big\{\left[E(^{12}\mathrm{Be}) + E(\mathrm{n}_1) + E(\mathrm{n}_2)\right]^2 \\ &\quad - \left[\boldsymbol{P}(^{12}\mathrm{Be}) + \boldsymbol{P}(\mathrm{n}_1) + \boldsymbol{P}(\mathrm{n}_2)\right]^2\Big\}^{1/2}, \quad (4) \end{aligned}$$

where $E(^{12}\mathrm{Be})$, $E(\mathrm{n}_1)$, $E(\mathrm{n}_2)$ are the total energy of the breakup fragment ^{12}Be and those of two neutrons respectively, and $\boldsymbol{P}(^{12}\mathrm{Be})$, $\boldsymbol{P}(\mathrm{n}_1)$, $\boldsymbol{P}(\mathrm{n}_2)$ denote the momenta of three breakup products respectively. The relative energy E_{rel} of the three outgoing particles is extracted from $M(^{14}\mathrm{Be}^{*})$ according to Eq. (3).

The studies of Coulomb breakup mechanism, correlation of two valent neutrons and the dineutron correlation depend on reduced transition probability B(E1) spectroscopy [4, 9, 31]. According to the semi-classical virtual photon model [18] based on first-order perturbation theory, the Coulomb breakup cross section is proportional to the E1 virtual photon number $N_{\rm E1}(\theta_{\rm cm}, E_x)$ and B(E1) spectrum as expressed by

$$\frac{{\rm d}^2\sigma}{{\rm d}\Omega_{\rm cm}{\rm d}E_{\rm rel}} = \frac{16\pi^3}{9\hbar c}\frac{{\rm d}N_{\rm E1}(\theta_{\rm cm}, E_x)}{{\rm d}\Omega_{\rm cm}}\frac{{\rm d}B({\rm E1})}{{\rm d}E_{\rm rel}}. \quad (5)$$

Therefore, the B(E1) spectrum containing nuclear structure can be extracted according to the experimental cross section.

5 Results and discussion

The investigation on RIB nuclear physics is based on reverse kinematics and the assumption of a thin target. Some experiments [9] have indicated a significant influence of experimental setup on energy spectroscopy. In the following we will discuss systematically the effects of the target thickness and detector performance behind the target on the experimental results.

5.1 Thin target approximation

Increasing the target thickness may enhance the reaction yield and allow research on nuclei close to the drip line. At the same time, it distorts the reconstructed relative energy spectrum shape. Fixing the incident energy as 35 MeV/u, the Coulomb breakup of ^{14}Be on a Pb target was simulated. Ignoring the influence from the performance of the detectors behind the target, the reconstructed relative energy spectra are displayed in Fig. 4(a). When the target thickness equals 0.1 mm, the relative energy spectrum is quite close to the real spectrum. As the target thickness increases, the spectrum peak position moves towards higher relative energy and the distribution becomes broader. Introducing the mean value $\mu_{\rm rel}$ and standard deviation $\sigma_{\rm rel}$, the variation of the spectrum with target thickness is shown in Fig. 4(b). In this plot the values of $\mu_{\rm rel}$ and $\sigma_{\rm rel}$ for a target thickness of 0.1 mm were taken as references, and what the vertical axis indicates are relative values. $\mu_{\rm rel}$ and $\sigma_{\rm rel}$ vary nonlinearly as the target thickness increases. $\mu_{\rm rel}$ and $\sigma_{\rm rel}$ increase rapidly when the target thickness is larger than ∼0.4 mm, i.e. the reconstructed relative energy spectrum is distorted much due to the increase in target thickness. In Fig. 4(c) and Fig. 4(d) we also present the corresponding B(E1) spectra of different target thicknesses. A similar dependence of B(E1) on target thickness is interpreted.

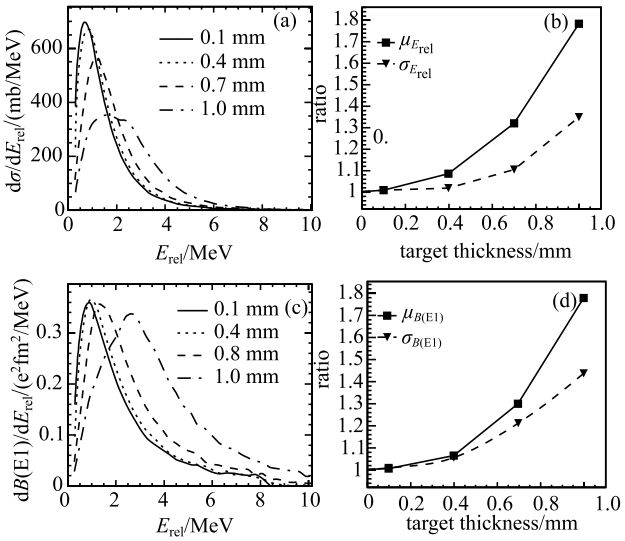

Fig. 4. (a) The relative energy spectra for different target thickness reconstructed by invariant mass method. (b) displays how the target thickness influence the mean value $\mu_{\rm rel}$ and standard deviation $\sigma_{\rm rel}$ of the relative energy spectrum. (c) and (d) indicate how the target thickness influences the B(E1) spectrum.

In the following, we will do some qualitative analysis for the target thickness influence on the relative energy spectrum. The effects of the finite target thickness include two aspects — the momentum change of the projectile ^{14}Be and that of the outgoing fragment ^{12}Be. The target thickness influence on the incident nucleus momentum is usually negligible in comparison with the effect due to the behind-target detectors. Hence, we focus on the target effects on the outgoing particles. According to Eq. (3), the relative energy spectrum only depends on the experiment outcome variable $M(^{14}{\rm Be}^*)$, which can be obtained by Eq. (4). Squaring Equation (4), we get the mass squared $M^2(^{14}{\rm Be}^*)$ of $^{14}{\rm Be}^*$ expression as follows

$$\begin{aligned} M^2(^{14}{\rm Be}^*) = &\sum_{i=1}^{3} M_i^2 - 2\left[P({\rm n}_1)P({\rm n}_2)\cos\theta_1 - E({\rm n}_1)E({\rm n}_2)\right] \\ &- 2\left[P({\rm n}_1)P(^{12}{\rm Be})\cos\theta_2 + P({\rm n}_2)P(^{12}{\rm Be})\cos\theta_3\right] \\ &+ 2\left[E({\rm n}_1)+E({\rm n}_2)\right]\left[M^2(^{12}{\rm Be}) + P^2(^{12}{\rm Be})\right]^{1/2}, \end{aligned} \quad (6)$$

where $\sum_{i=1}^{3} M_i^2$ is the sum of the mass squared of the three outgoing particles; θ_1, θ_2 and θ_3 are the angles between the two neutrons as well as those between the two neutrons and ^{12}Be respectively. Eq. (6) indicates that the target affects the relative energy by changing the ^{12}Be momentum of $\boldsymbol{P}(^{12}{\rm Be})$, which may be decomposed into the momentum value $P(^{12}{\rm Be})$ and the angles θ_2 and θ_3. The change of $P(^{12}{\rm Be})$ after it is created in the target

equals the energy deposition of ^{12}Be in the target, which can be briefly analyzed by the energy deposition theory of ions. According to the Bethe-Block formula there is approximately $\Delta E_k \propto \Delta x z^2/(E_k/A)$, where Δx is the medium thickness; z and E_k/A are the atomic number and kinetic energy per nucleon of an incident nucleus respectively. With the type of a projectile and incident energy fixed, an increase of target thickness Δx will make the energy difference increase linearly. At the same time, the scattering angle becomes larger according to Rutherford scattering theory. That is why the parameters indicating the spectrum distortion increases non-linearly with the target thickness. By simulation we also find that experiments with higher energy per nucleon may tolerate a thicker target, which is also consistent with the qualitative analysis based on the Bethe-Block formula.

5.2 Neutron detector performances

According to the simulation, the performance of the charged ion telescope today does not have a significant influence on the spectroscopic study of the Coulomb breakup of ^{14}Be on a Pb target. Hence, the neutron wall performance effects have been thoroughly analyzed. If the detection efficiency for events with certain relative energy is extremely low, there will be poor statistics in the experiment, which may cause incorrect understanding of the nuclear structure. For different experimental settings Fig. 5 exhibits the calculated efficiency curves of neutron walls, where the problem of two-neutron cross talk [30] was not considered. The efficiency varies with the relative energy as shown by the solid line when the angular acceptance is 4° (half angle) in the x and y directions and the incident energy of ^{14}Be is 35 MeV/u. It is quite similar to that of the neutron wall at MSU used in the experiment in Ref. [32], with a very low efficiency especially for high relative energy. Keeping the same experimental setting but doubling the angular coverage to 8°, there is an apparent rise in efficiency as shown by the dashed line. For different incident energy the neutron wall also manifests different characteristics of efficiency variation. The higher the incident energy the more forward the outgoing neutrons, which will enhance the efficiency of a neutron wall with certain angular acceptance. At the same time, there will be more events with two neutrons hitting on the same scintillator bar. Hence, the efficiency drops at low relative energy, which is indicated in Fig. 5(b) with an incident energy of 280 MeV/u. The regular fluctuations of the efficiency curve are due to the non-compact configuration of the scintillator bars.

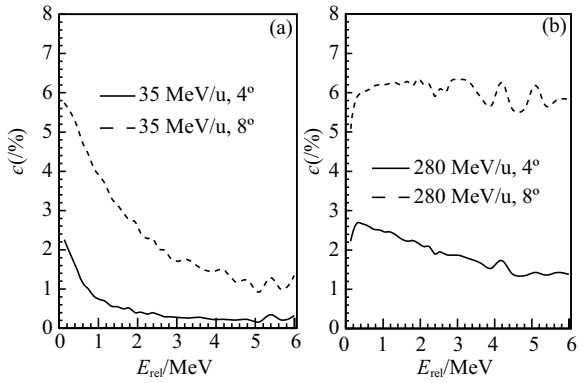

Fig. 5. The neutron wall efficiency (ε) curves for different experiment design of ^{14}Be+Pb given by the simulation. The incident energy of ^{14}Be is 35 MeV/u in (a) and 280 MeV/u in (b).

6 Conclusions

A two-body model (^{12}Be+dineutron) was implemented to describe the 2n halo nucleus ^{14}Be and the three-body CDCC calculation was used successfully in the ^{14}Be breakup reactions on a Pb target. This indicates that the three-body CDCC calculation is fit for the description of the breakup of 2n halo nuclei in the given scenario. Combining the theoretical calculation with the Geant4 toolkit, a simulation workspace for the kinematically complete measurement of ^{14}Be Coulomb breakup was developed. By the simulation it was found that the relative energy spectrum is very sensitive to the target thickness in heavy target Coulomb excitation experiments. For the detectors behind the target, the neutron wall substantially affects the uncertainty of the energy spectroscopy. Then, it was discussed how the angular acceptance and the incident energy influence the neutron wall efficiency. The corresponding results can be used as references for Coulomb breakup research for other neutron halo nuclei.

We thank our collaborators from Peking University and the Institute of Modern Physics for their helpful suggestions. Thanks also go to Dr. Pang and Dr. Moro for their help in FRESCO usage.

References

1 I. Tanihata, H. Hamagaki, O. Hashimoto et al, Phys. Rev. Lett., **55**: 2676–2679 (1985)
2 Y.G. Ma, D.Q. Fanga , X.Y. Sun et al, Phys. Lett. B, **743**: 306–309 (2015)
3 N. A. Orr, N. Anantaraman, Sam M. Austin et al, Phys. Rev. Lett., **69**: 2050–2053 (1992)
4 N. Fukuda, T. Nakamura, N. Aoi et al, Phys. Rev. C, **70**: 054606 (2004)
5 Cheng TAO, Yugang MA, Guoqiang ZHANG et al, Nucl. Sci. Tech., **24**: 030502 (2013)
6 Ning Yu, Enrico Maglione and Lidia Ferreira, Nucl. Sci. Tech., **24**: 050517 (2013)
7 T. Nakamura, N. Fukuda, N. Aoi et al, Phys. Rev. C, **79**: 035805 (2009)
8 J. Wang, A. Galonsky, J. J. Kruse et al, Phys. Rev. C, **65**: 034306 (2002)
9 T. Nakamura, A. M. Vinodkumar,T. Sugimoto et al, Phys. Rev. Lett, **96**: 252502 (2006)
10 M. Labiche, N. A. Orr, F. M. Marqués et al, Phys. Rev. Lett, **86**: 600–603 (2001)
11 J. Allison, Univ. Manchester, K. Amako et al, IEEE Tran. Nucl. Sci., **53**: 270–278 (2006)
12 Zhongzhou Ren, Gongou Xu, Phys. Lett. B., **252**: 311–313 (1990)
13 T. Matsumoto, T. Egami, K. Ogata et al, Phys. Rev. C, **73**: 051602(R) (2006)
14 M. Rodriguez-Gallardo, J. M. Arias, Gómez-Camacho et al, Phys. Rev. C, **77**: 064609 (2008)
15 K. Hagino, H. Sagawa, Phys. Rev. C, **72**: 044321 (2005)
16 Maria Colonna, Virgil Baran, Stefano Burrello et al, Nucl. Sci. Tech., **26**: s20509 (2013)
17 N. Austern, Y. Iseri, M. Kamimura et al, Phys. Rep., **154**: 125 (1987)
18 C. A. Bertulani, G. Baur, Phys. Rep., **163**: 299 (1988)
19 K. Rusek, I. Martel, J. Gómez-Camacho et al, Phys. Rev. C, **72**: 037603 (2005)
20 Yoshiko Kanada-Enyo, Phys. Rev. C, **76**: 044323 (2007)
21 K. Rusek, N. Alamanos, N. Keeley et al, Phys. Rev. C, **70**: 014603 (2004)
22 T. Suzuki, R. Kanungo, O. Bochkarev et al, Nucl. Phys. A, **658**: 313–326 (1999)
23 I. J. Thompson, M. V. Zhukov, Phys. Rev. C, **53**: 708–714 (1996)
24 T. Sugimoto, T. Nakamura, Y. Kondo et al, Phys. Lett. B, **654**: 160–164 (2007)
25 M. Buenerd, A. Lounis, J. Chauvin et al, Nucl. Phys. A, **424**: 313–334 (1984)
26 G. Duhamel, L. Marcus, H. Langevin-Joliot et al, Nucl. Phys. A, **174**: 485–496 (1971)
27 M. Wang, G. Audi, A. H. Wapstra et al, Chin. Phys. C, **36**: 1603 (2012)
28 M. Vilches, S. García-Pareja, R. Guerrero et al, Nucl. Instrum. Methods B, **254**: 219 (2007)
29 Yu-Shou Song, Yan-Lin Ye, Yu-Cheng Ge et al, Chinese Physics C, **33**: 860–865 (2009)
30 Haibo You, Yushou Song, Jun Xiao et al, Plasma Sci. and Tech., **14**: 473–477 (2012)
31 M. A. Nagarajan, S.M. Lenzi, A. Vitturi, Eur. Phys. J. A, **24**: 63 (2005)
32 D. Sackett, K. Ieki, A. Galonsky et al, Phys. Rev. C, **48**: 118 (1993)